

Precision sparticle spectroscopy in the inclusive same-sign dilepton channel at LHC

Konstantin T. Matchev¹, Filip Moortgat², Luc Pape², and Myeonghun Park¹

¹*Physics Department, University of Florida, Gainesville, FL 32611, USA and*

²*ETHZ, Zurich, Switzerland*

(Dated: 27 July, 2010)

The inclusive same-sign dilepton channel is already recognized as a promising discovery signature for supersymmetry in the early days of the LHC. We point out that it can also be used for precision *measurements* of sparticle masses after the initial discovery. As an illustration, we consider the LM6 CMS study point in minimal supergravity, where the same-sign leptons most often result from chargino decays to sneutrinos. We discuss three different techniques for determining the chargino and sneutrino masses *in an inclusive manner*, i.e. using *only* the two well measured lepton momenta, while treating all other upstream objects in the event as a single entity of total transverse momentum \vec{P}_T . This approach takes full advantage of the large production rates of colored superpartners, but does not rely on the poorly measured hadronic jets, and avoids any jet combinatorics problems. We discuss the anticipated precision of our methods in the early LHC data.

PACS numbers: 14.80.Ly, 12.60.Jv, 11.80.Cr

A long standing problem in hadron collider phenomenology has been the determination of the absolute mass scale of new particles in events with missing energy. The prototypical example of this sort is provided by any model of low-energy supersymmetry (SUSY) with conserved R -parity, in which the lightest superpartner (LSP), typically the lightest neutralino $\tilde{\chi}_1^0$, is a neutral, weakly interacting particle of a priori unknown mass [1]. Astrophysics also adds credence to such scenarios, since the LSP is a potential dark matter candidate, whose relic abundance is typically in the right ballpark [2]. R -parity conservation guarantees that every event contains (at least) two invisible particles, whose energies and momenta are not measured, making the full reconstruction of such events a very challenging task.

Recently, several solutions to this problem at the Large Hadron Collider (LHC) have been proposed. Most of them rely on exclusive channels [3], where a sufficiently long decay chain can be properly identified. Unfortunately, this almost inevitably requires the use of hadronic jets in some form in the analysis – in most SUSY models, the main LHC signal is due to the strong production of colored superpartners, whose cascade decays to the neutral LSP necessarily involve hadronic jets. For many reasons, jets are notoriously difficult to deal with, especially in a hadron collider environment. Because of the high jet multiplicity in SUSY signal events, any jet-based analysis is bound to face a severe combinatorial problem and is unlikely to achieve any good precision. Thus it is imperative to have alternative methods which avoid the direct use of jets and instead rely only on the well measured momenta of any (isolated) leptons in the event.

In this letter, we describe three such methods, which are free of the jet combinatorial problem. For illustration, we shall use the standard example of R -parity conserving supersymmetry with a $\tilde{\chi}_1^0$ LSP. Its collider signatures have been extensively studied, and typically involve jets, leptons and missing transverse energy [1]. Among those, the inclusive same-sign dilepton channel has already been

TABLE I: Selected sparticle masses (in GeV) at point LM6. We list the average \tilde{q}_L mass $M_{\tilde{q}_L} = \frac{1}{2}(M_{\tilde{u}_L} + M_{\tilde{d}_L})$.

$M_{\tilde{g}}$	$M_{\tilde{q}_L}$	$M_{\tilde{\chi}_1^+}$	$M_{\tilde{\nu}_\ell}$	$M_{\tilde{\nu}_\ell}$	$M_{\tilde{\chi}_1^0}$
939.8	862	305.3	291.0	275.7	158.1

identified as a unique opportunity for an early SUSY discovery at the LHC [4, 5]. The two leptons of the same charge can be easily triggered on, and provide a good handle for suppressing the SM background. In our analysis we use the LM6 CMS study point [4], whose relevant mass spectrum is given in Table I. At point LM6, signal events with two isolated same-sign leptons typically arise from the SUSY event topology in Fig. 1. Consider the inclusive production of same-sign charginos, which decay leptonically as shown in the yellow-shaded box in the figure. The resulting sneutrino ($\tilde{\nu}_\ell$) could be the LSP itself, or, as in the case of LM6, may further decay invisibly to a neutrino ν and the true LSP $\tilde{\chi}_1^0$. Such same-sign chargino pairs typically result from squark decays, as indicated in Fig. 1. In turn, the squarks may be produced directly through a t -channel gluino exchange, or indirectly in gluino decays. Note that the two same-sign leptons in Fig. 1 are accompanied by a number of upstream objects (typically jets) which may originate from various sources, e.g. initial state radiation, squark decays, or decays of even heavier particles up the decay chain. In order to stay clear of jet combinatorial issues, we shall adopt a fully inclusive approach to the same-sign dilepton signature, by treating all the upstream objects within the black rectangular frame in Fig. 1 as a single entity of total transverse momentum \vec{P}_T .

Given this very general setup, we now pose the following question: assuming that a SUSY discovery is made in the inclusive same-sign dilepton channel, is it possible to measure the *individual* sparticle masses M_p and M_c involved in the leptonic decays of Fig. 1, using only the

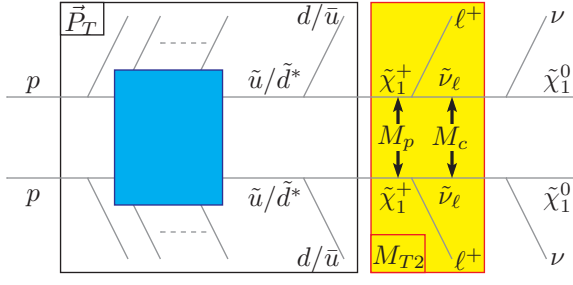


FIG. 1: The typical SUSY event topology producing two isolated same-sign leptons at point LM6 (see text for details). The diagram for a pair of negatively charged leptons $\ell^- \ell^-$ is analogous.

transverse momenta of the two leptons $\vec{p}_{\ell T}^{(1)}$ and $\vec{p}_{\ell T}^{(2)}$, and the *total* upstream transverse momentum \vec{P}_T ? Although it may appear that those three vectors do not provide a lot of information to go on, we shall show that this is possible. We discuss three different approaches.

Method I. Let us concentrate directly on the observed lepton momenta $\vec{p}_{\ell T}^{(i)}$. Consider the two collinear momentum configurations illustrated in Fig. 2 and defined as follows. In each configuration, the lepton momenta are the same: $\vec{p}_{\ell T}^{(1)} = \vec{p}_{\ell T}^{(2)}$; and then they can be either parallel or anti-parallel to the measured upstream \vec{P}_T :

$$s = +1 \Rightarrow \vec{p}_{\ell T}^{(1)} = \vec{p}_{\ell T}^{(2)} \uparrow \vec{P}_T; \quad (1)$$

$$s = -1 \Rightarrow \vec{p}_{\ell T}^{(1)} = \vec{p}_{\ell T}^{(2)} \updownarrow \vec{P}_T. \quad (2)$$

In what follows we shall use the integer $s = +1$ ($s = -1$) to refer to the parallel (anti-parallel) configuration: $s \equiv \cos(\vec{p}_{\ell T}^{(1)}, \vec{P}_T) = \cos(\vec{p}_{\ell T}^{(2)}, \vec{P}_T)$. Now let us measure the *maximum* lepton momentum in each configuration:

$$p_{\ell T}(sP_T) \equiv \max_{\vec{p}_{\ell T}^{(1)} = \vec{p}_{\ell T}^{(2)} \wedge \cos(\vec{p}_{\ell T}^{(1)}, \vec{P}_T) = s} \left\{ p_{\ell T}^{(i)} \right\}. \quad (3)$$

Observe that *both* $p_{\ell T}(+P_T)$ and $p_{\ell T}(-P_T)$ can be directly measured from the lepton p_T distributions. For example, construct a 2D scatter plot $\{x, y\}$ of

$$x = \cos(\vec{p}_{\ell T}^{(1)} + \vec{p}_{\ell T}^{(2)}, \vec{P}_T), \quad y = |\vec{p}_{\ell T}^{(1)} + \vec{p}_{\ell T}^{(2)}|, \quad (4)$$

with the cut $|\vec{p}_{\ell T}^{(1)} - \vec{p}_{\ell T}^{(2)}| < \epsilon$ (~ 0), and take the limit

$$p_{\ell T}(sP_T) = \lim_{x \rightarrow s} \left(\frac{y}{2} \right). \quad (5)$$

Armed with the two measurements $p_{\ell T}(+P_T)$ and $p_{\ell T}(-P_T)$, we can now directly solve for the masses M_p and M_c . The formula for $p_{\ell T}(sP_T)$ is

$$p_{\ell T}(sP_T) = \frac{M_p^2 - M_c^2}{4M_p^2} \left(\sqrt{4M_p^2 + (sP_T)^2} - sP_T \right). \quad (6)$$

Inverting (6), we get

$$M_p = \frac{\sqrt{p_{\ell T}(-P_T) p_{\ell T}(+P_T)}}{p_{\ell T}(-P_T) - p_{\ell T}(+P_T)} P_T, \quad (7)$$

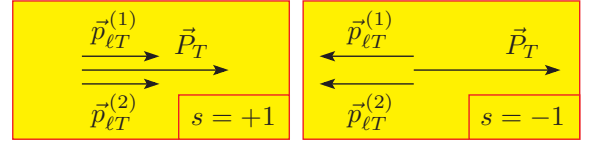


FIG. 2: The two special momentum configurations defined in eqs. (1,2).

thus fixing the *absolute* mass scale in the problem. Once the parent mass M_p is known, the child mass M_c is

$$M_c = M_p \sqrt{1 - 2 \frac{p_{\ell T}(-P_T) - p_{\ell T}(+P_T)}{P_T}}. \quad (8)$$

Thus we found the true sparticle masses M_p and M_c directly in terms of the measured lepton momenta $p_{\ell T}(\pm P_T)$ and upstream momentum P_T . Note that the choice of the *value* for P_T in eqs. (7) and (8) is arbitrary, which can be used to our advantage, e.g. to select the most populated P_T bin, minimizing the statistical error.

Method II. In our previous method, the lepton momenta $p_{\ell T}(\pm P_T)$ were measured directly from the data as implied by eq. (5). Alternatively, we can obtain them indirectly from the endpoint of the Cambridge M_{T2} variable [6]. To be more precise, we apply the “subsystem” M_{T2} variable introduced in [7] to the purely leptonic subsystem in the yellow-shaded box of Fig. 1. Following the generic notation of Ref. [7], we denote the input (test) mass of the sneutrino child as \tilde{M}_c . The subsystem M_{T2} variable is now defined as follows. First form the transverse mass M_T for each (chargino) parent

$$M_T^{(i)} \equiv \sqrt{\tilde{M}_c^2 + 2 \left(|\vec{p}_{\ell T}^{(i)}| \sqrt{\tilde{M}_c^2 + |\vec{p}_{cT}^{(i)}|^2} - \vec{p}_{\ell T}^{(i)} \cdot \vec{p}_{cT}^{(i)} \right)}$$

in terms of the assumed test mass \tilde{M}_c and transverse momentum $\vec{p}_{cT}^{(i)}$ for each (sneutrino) child. Just like the traditional M_{T2} [6], the leptonic subsystem M_{T2} variable [7] is defined through a minimization procedure over all possible partitions of the unknown children momenta $\vec{p}_{cT}^{(k)}$, consistent with transverse momentum conservation $\sum_k (\vec{p}_{cT}^{(k)} + \vec{p}_{\ell T}^{(k)}) + \vec{P}_T = 0$

$$M_{T2}(\tilde{M}_c, \vec{P}_T, \vec{p}_{\ell T}^{(i)}) \equiv \min \left\{ \max \left\{ M_T^{(1)}, M_T^{(2)} \right\} \right\}. \quad (9)$$

The M_{T2} distribution has an upper kinematic endpoint

$$M_{T2}^{max}(\tilde{M}_c, P_T) \equiv \max_{\text{all events}} \left\{ M_{T2}(\tilde{M}_c, \vec{P}_T, \vec{p}_{\ell T}^{(i)}) \right\}, \quad (10)$$

which can be experimentally measured and subsequently interpreted as the corresponding parent mass \tilde{M}_p

$$\tilde{M}_p(\tilde{M}_c, P_T) \equiv M_{T2}^{max}(\tilde{M}_c, P_T), \quad (11)$$

providing one functional relationship among \tilde{M}_p and \tilde{M}_c , but leaving the individual masses still to be determined.

For us the importance of the M_{T2} variable (9) is that the momentum configurations in Fig. 2 are precisely the ones which determine its endpoint M_{T2}^{max} . The complete analytical dependence of the M_{T2} endpoint $\tilde{M}_p(\tilde{M}_c, P_T)$ on *both* of its arguments \tilde{M}_c and P_T is now known [7]:

$$\tilde{M}_p(\tilde{M}_c, P_T) = \begin{cases} \tilde{M}_p(\tilde{M}_c, +P_T), & \text{if } \tilde{M}_c \leq M_c, \\ \tilde{M}_p(\tilde{M}_c, -P_T), & \text{if } \tilde{M}_c \geq M_c, \end{cases} \quad (12)$$

where

$$\tilde{M}_p(\tilde{M}_c, sP_T) = \left\{ \left[p_{\ell T}(sP_T) + \sqrt{\left(p_{\ell T}(sP_T) + \frac{sP_T}{2} \right)^2 + \tilde{M}_c^2} \right]^2 - \frac{(sP_T)^2}{4} \right\}^{\frac{1}{2}}. \quad (13)$$

Thus we can alternatively obtain the sparticle masses by measuring just two M_{T2} kinematic endpoints, with arbitrary choices for the test mass \tilde{M}_c and the upstream P_T . For concreteness, let us pick some fixed \tilde{M}'_c and P'_T , form the corresponding M_{T2} distribution (9) and measure its endpoint \tilde{M}'_p , also making a note of the configuration s' :

$$\left\{ \tilde{M}'_c, P'_T \right\} \xrightarrow{\text{measure}} \left\{ \tilde{M}'_p, s' \right\}. \quad (14)$$

Now perform a second such measurement

$$\left\{ \tilde{M}''_c, P''_T \right\} \xrightarrow{\text{measure}} \left\{ \tilde{M}''_p, s'' \right\}. \quad (15)$$

By inverting (13), these two measurements allow the experimental determination of

$$p_{\ell T}(s'P'_T) = \frac{\tilde{M}'_p{}^2 - \tilde{M}'_c{}^2}{4\tilde{M}'_p{}^2} \left(\sqrt{4\tilde{M}'_p{}^2 + (s'P'_T)^2} - s'P'_T \right) \quad (16)$$

and similarly for $p_{\ell T}(s''P''_T)$. Now taking the ratio

$$r \equiv \frac{p_{\ell T}(s'P'_T)}{p_{\ell T}(s''P''_T)} = \frac{\sqrt{4\tilde{M}'_p{}^2 + (s'P'_T)^2} - s'P'_T}{\sqrt{4\tilde{M}'_p{}^2 + (s''P''_T)^2} - s''P''_T}, \quad (17)$$

where in the second step we used eq. (6), we can solve (17) for the *true* parent mass M_p in terms of measured quantities:

$$M_p = \left\{ \frac{-rs'P'_T s''P''_T}{(1-r^2)^2} \left(r - \frac{s'P'_T}{s''P''_T} \right) \left(r - \frac{s''P''_T}{s'P'_T} \right) \right\}^{\frac{1}{2}}, \quad (18)$$

and then find the *true* child mass M_c from (6) as

$$M_c = M_p \left[1 - \left(1 - \frac{\tilde{M}'_c{}^2}{\tilde{M}'_p{}^2} \right) \frac{\sqrt{4\tilde{M}'_p{}^2 + (s'P'_T)^2} - s'P'_T}{\sqrt{4M_p^2 + (s'P'_T)^2} - s'P'_T} \right]^{\frac{1}{2}} \quad (19)$$

with M_p already given by (18). Note that in this method, the values of \tilde{M}'_c , \tilde{M}''_c , P'_T and P''_T can be chosen at will, allowing for repeated measurements of M_p and M_c .

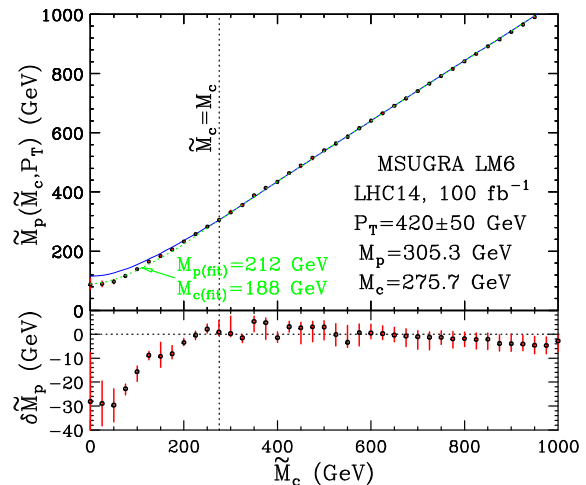


FIG. 3: M_{T2}^{max} versus the test mass \tilde{M}_c , as obtained in our simulations (data points) from a sample with $P_T = 420 \pm 50$ GeV, or theoretically from eq. (12) (blue solid line), as well as their difference (lower panel).

Method III. The third and final method for extracting the two masses M_p and M_c will make use of the celebrated “kink” in the M_{T2} endpoint function (12) [8]. Since $\tilde{M}_p(\tilde{M}_c, +P_T)$ and $\tilde{M}_p(\tilde{M}_c, -P_T)$ have different slopes at the crossover point $\tilde{M}_c = M_c$, the function $\tilde{M}_p(\tilde{M}_c, P_T)$ has a slope discontinuity precisely at the correct value M_c of the child mass, providing an alternative measurement of the absolute mass scale [8]. The procedure is illustrated in Fig. 3 for the LM6 study point of Table I. The blue solid line shows the theoretically expected shape from eq. (12), for $P_T = 420$ GeV, which is roughly the mean of the P_T distribution at point LM6. In the LM6 case the kink is very mild, only 3.3° [7].

In order to test the precision of the three methods, we perform event simulations using the PYTHIA event generator [9] and PGS detector simulation [10]. We consider the LHC at its nominal energy of 14 TeV and 100 fb^{-1} of data. To ensure discovery, we use standard CMS cuts as follows [4, 11]: exactly two isolated leptons with $p_T > 10$ GeV, at least three jets with $p_T > (175, 130, 55)$ GeV, $\cancel{E}_T > 200$ GeV and a veto on tau jets. With those cuts, in the dimuon channel alone, the remaining SM background cross-section is rather negligible (0.15 fb), while the SUSY signal is 14 fb, already leading to a 22σ discovery with just 10 fb^{-1} of data [4, 11]. In order to compare to the theoretical result in Fig. 3, we select a ± 50 GeV P_T bin around $P_T = 420$ GeV and construct a series of M_{T2} distributions, for different input values of \tilde{M}_c . For each case, we include all SM and SUSY combinatorial backgrounds, and extract the M_{T2}^{max} endpoint by a linear unbinned maximum likelihood fit, obtaining the data points shown in Fig. 3. We see that the M_{T2} endpoint can be determined rather well ($\delta\tilde{M}_p \lesssim 3$ GeV), but *only* on the right branch $\tilde{M}_c \geq M_c$. In contrast, the M_{T2} endpoints on the left branch $\tilde{M}_c \leq M_c$ are considerably un-

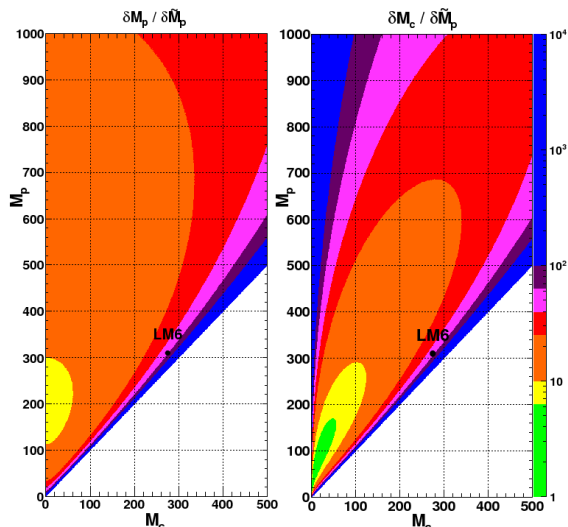


FIG. 4: Scaling factors relating the error $\delta\tilde{M}_p$ in the extraction of the M_{T2} endpoint to the resulting uncertainties δM_p and δM_c on the parent and child masses calculated from (18) and (19), as a function of the true input masses M_c and M_p .

derestimated, washing out the expected kink. There are two separate reasons behind this effect. Recall that the M_{T2} endpoint on the left branch is obtained in the configuration $s = +1$ of Fig. 2, which requires the lepton to be emitted in the backward direction. As a result, the parent boost favors configurations with $s \simeq -1$ over $s \simeq +1$. Another consequence is that leptons with $s \simeq +1$ are softer and more easily rejected by the offline p_T cuts. We conclude that M_{T2}^{max} measurements on the left branch are in general not very reliable, and tend to jeopardize the traditional kink method. For example, using Method III to fit the data in Fig. 3 (green dotted line), we find best fit values of only $M_{p(fit)} = 212$ GeV and $M_{c(fit)} = 188$ GeV. Method I has a similar problem, since $p_{\ell T}(+P_T)$ is measured from events in the $s = +1$ configuration. Using the \tilde{M}_p measurements from Fig. 3 at $\tilde{M}_c = 0$ and $\tilde{M}_c = 1$ TeV, we find from eq. (16) that $p_{\ell T}(+420 \text{ GeV}) = 8.8$ GeV and $p_{\ell T}(-420 \text{ GeV}) = 50.6$ GeV (compare to the

nominal values of 14.8 GeV and 53.6 GeV, correspondingly). The resulting mass determination via eqs. (7,8) is $M_{p(fit)} = 212$ GeV and $M_{c(fit)} = 190$ GeV. We see that in both Method I and Method III, the masses are underestimated due to the systematic underestimation of the left M_{T2}^{max} branch in Fig. 3. It is therefore of great interest to have an alternative method, which relies on the right M_{T2}^{max} branch alone.

This is where the available freedom in Method II comes into play, since *both* test masses \tilde{M}'_c and \tilde{M}''_c can be chosen on the right branch. Taking $P'_T = 350 \pm 50$ GeV and $P''_T = 500 \pm 50$ GeV and repeating our earlier analysis, we find that $\delta\tilde{M}_p$ on the right branch is still on the order of 3 GeV, as in Fig. 3. The resulting error δM_p (δM_c) on the measured parent (child) mass can be easily propagated from eqs. (18,19). The two ratios $\delta M_p/\delta\tilde{M}_p$ and $\delta M_c/\delta\tilde{M}_p$ are shown in Fig. 4, where for concreteness we have taken $\tilde{M}'_c = \tilde{M}''_c = 1000$ GeV. Fig. 4 reveals that the LM6 input values of M_c and M_p are rather unlucky, since the error $\delta\tilde{M}_p$ on the M_{T2} endpoint is then amplified by a factor of almost 70. However, if M_c and M_p happened to be different, with the rest of the spectrum the same, the precision quickly improves. For example, with $\delta\tilde{M}_p = \pm 3$ GeV, the masses can be determined to within ± 30 GeV (± 75 GeV) within the yellow (orange) region. One should keep in mind that the dominant uncertainty on $\delta\tilde{M}_p$ is due to the SUSY combinatorial background. We have verified that in the absence of such combinatorial background, $\delta\tilde{M}_p \lesssim 1$ GeV and the typical precision on M_p and M_c from Fig. 4 is then at the level of 10%.

In conclusion, we considered the inclusive same-sign dilepton channel in SUSY, which so far has only been used for discovery, but not for mass measurements. We demonstrated that it allows a separate determination of the chargino and sneutrino masses. We discussed three different methods, which rely exclusively on the well measured lepton momenta. The methods are completely general and inclusive, and can be applied to other SUSY topologies and to non-SUSY scenarios like UED [12].

Acknowledgements. The work of KM and MP is supported by a US DoE grant DE-FG02-97ER41029.

-
- [1] See, e.g. D. Chung *et al.*, Phys. Rept. **407**, 1 (2005).
 - [2] See, e.g. G. Bertone, D. Hooper and J. Silk, Phys. Rept. **405**, 279 (2005).
 - [3] For recent studies on the three classic methods, see H.-C. Cheng, J. F. Gunion, Z. Han and B. McElrath, Phys. Rev. D **80**, 035020 (2009); K. Matchev, F. Moortgat, L. Pape and M. Park, JHEP **0908**, 104 (2009); A. Barr, B. Gripaios and C. Lester, arXiv:0908.3779 [hep-ph], and references therein.
 - [4] G. L. Bayatian *et al.*, J. Phys. G **34**, 995 (2007).
 - [5] G. Aad *et al.*, arXiv:0901.0512 [hep-ex].
 - [6] C. G. Lester and D. J. Summers, Phys. Lett. B **463**, 99 (1999); A. Barr, C. Lester and P. Stephens, J. Phys. G **29**, 2343 (2003).
 - [7] M. Burns, K. Kong, K. T. Matchev and M. Park, JHEP **0903**, 143 (2009).
 - [8] W. S. Cho, K. Choi, Y. G. Kim and C. B. Park, Phys. Rev. Lett. **100**, 171801 (2008); JHEP **0802**, 035 (2008); B. Gripaios, JHEP **0802**, 053 (2008); A. J. Barr, B. Gripaios and C. G. Lester, JHEP **0802**, 014 (2008).
 - [9] T. Sjostrand, S. Mrenna and P. Skands, JHEP **0605**, 026 (2006).
 - [10] <http://www.physics.ucdavis.edu/~conway/research/software/pgs/pgs4-general.htm>
 - [11] Yu. Pakhotin *et al.*, CERN-CMS-NOTE-2006-134.
 - [12] T. Appelquist, H. C. Cheng and B. A. Dobrescu, Phys. Rev. D **64**, 035002 (2001); H. C. Cheng, K. T. Matchev and M. Schmaltz, Phys. Rev. D **66**, 056006 (2002).